JOURNAL OF COMPUTATIONAL PHYSICS 29, 173–198 (1978)

Calculation of Three-Dimensional Stationary Supersonic Flow Fields by Applying the "Progonka" Process to a Conservative Formulation of the Governing Equations

C. WEILAND

Deutsche Forschungs- und Versuchsanstalt für Luft- und Raumfahrt, 5 Köln 90, Linder Höhe, Germany

Received March 1, 1977; revised September 14, 1977

Stationary three-dimensional inviscid flow fields past bodies with a blunt or pointed nose are calculated for supersonic Mach numbers. The equations of motion are discretized such that it is possible to calculate the intensity and location of embedded shocks with high accuracy. For this purpose, the dependent variables of the system of differential equations must be used in conservative form. However, we do not apply the divergence form of the system of differential equations, but a vector–matrix form which allows us to solve the finite-difference equations by the use of the "progonka" process. By means of one-dimensional nonstationary examples, the accuracy which can be gained in the treatment of embedded shocks is tested using either conservative or nonconservative formulations of the equations of motion. It is seen that surprisingly good results can be achieved with the formulation chosen in this paper. Solutions of some selected flow fields are given which contain compression and expansion zones as well as embedded shocks. A comparison with experimental data, insofar as they are available, shows very good agreement.

1. INTRODUCTION

Today, we can choose among a considerable number of discrete numerical methods (finite-difference methods) for calculating three-dimensional inviscid supersonic flow fields. The use of integral and characteristics methods for three-dimensional problems seems, on the one hand, to involve too much effort and, on the other hand, to have limited application. As far as the author knows, none of these methods has been employed for the treatment of general three-dimensional inviscid flow fields with embedded shocks. The system of partial differential equations for these flows is almost exclusively solved by means of finite-difference algorithms.

A great variety of difference algorithms exists, and very frequently they are adjusted to the specific problem to be treated. When supersonic flows pass around blunt or pointed bodies, subsonic regions and embedded shocks with unknown shape and location can occur in the flow field to be calculated as a function of the Mach number M_∞, the angle of attack α, and the body geometry. Besides the treatment of the bow shock, these are the principal difficulties which must be solved by the difference method used in each case.

0021-9991/78/0292-0173$02.00/0

If a flow passes around a blunt body with Mach numbers $M_\infty > 1$, a subsonic region arises between body contour and detached shock wave (bow shock), which downstream becomes a supersonic region again. If we assume that the flow is stationary, then the differential equations which describe the subsonic region are of elliptic type and we obtain a boundary-value problem. However, since the boundaries are not completely known, e.g., the bow shock is to be determined during the calculation process, the solution of the boundary-value problem is difficult. References [1, 2] show a possible method of solving the above problem, known as the "inverse method." In this method, the associated body contour is calculated for a given shock contour in an iterative process. This is not very satisfactory, however, as it is very difficult to calculate the flow around an arbitrary body shape in this way. But if we take nonstationary differential equations and consider the time-asymptotic behavior at stationary boundary conditions as the desired solution, the differential equation system is of hyperbolic type. The initial boundary-value problem that arises contains the shock contour function as an unknown variable. A disadvantageous effect is exerted by the fourth independent variable—the time coordinate t—which substantially increases the formulation effort and the computing time. Nevertheless, the time-dependent method has found general acceptance, as can be seen from [3–7]. Localizing the bow shock is another problem, which in all recent papers [3–14] has been solved by means of a coordinate transformation which describes the bow shock and body contour by coordinate surfaces $\xi = \text{const}$. Further difficulties are associated with the treatment of embedded shocks. As is known, the governing equations can be written in strong conservative, weak conservative [15, 16], and nonconservative form. With the equations in nonconservative form, embedded shocks can only be computed very inaccurately if no additional effort is spent. In [17] embedded shocks, whose point of generation is given by the body geometry (jump in the first or second derivativeof the countour function), are calculated by means of the "shock-fitting" technique [18]. If the body contour function does not provide any information on the generation of an embedded shock, the shock is determined [17] by a combination of characteristics and Rankine–Hugoniot equations. Another possible way of computing embedded shocks with nonconservative equations is to introduce artificial dissipation terms [8]. However, since the required quantity of the artificial dissipation terms depends on the intensity of the shock, the solution in the shock-free flow field may be distorted accordingly.

Lax shows [19] that shocks can be calculated with a conservative formulation of the equations of motion. Departing from the system of equations in [19], shocks which are embedded in the flow field can be determined without any special treatment (shock-capturing technique), as is demonstrated in [20, 21].

In the region of shock formation the flow field variables show oscillations which can be attenuated by the introduction of appropriate artificial dissipation terms. In [22], the exact location of the shock is found by means of an additional interpolation prescription. For three-dimensional problems, Kutler [23–25] has applied the shock-capturing technique with great success.

Another very important problem is the treatment of the boundary conditions and/or

the calculation of the flow variables at the boundary. In the initial boundary-value problem here, the specific solution sought is determined by the boundary values—in addition to the initial values. Therefore the accuracy of the solution will depend just on the accuracy to which the boundary values can be calculated. A distinction is made between boundaries which are permeable (bow shock) or impermeable (body surface) for the flow medium. In [3, 5, 8, 14] the calculation of the flow variables on the boundaries is carried out with the same difference algorithm used to determine the variables in the field. This calculation is feasible, since the equations of the boundary conditions are contained in the solution algorithm which simultaneously computes the field variables along a line from the body to the bow shock. In the Russian literature, this method is called the "progonka" process. With it, all variables, in the field and on the boundaries, are computed with the same accuracy. A variety of further ways of treating the boundary conditions is discussed in [23, 26].

All these procedures, such as the reflection technique, the wave corrector technique [26], or the use of one-sided difference approximations, have in common the fact that the calculation of the flow variables on the boundaries and the calculation of those in the field are done with different accuracy. For example, the truncation errors of higher order are of different sizes, depending on whether central or one-sided difference approximations are used. In [7], a large system of interpolations and extrapolations is required to calculate the bow shock location, which of course impairs the accuracy.

To achieve as high an accuracy as possible, the flow variables on the boundaries and in the field are calculated in the present method by means of the progonka process. Furthermore, the equations of motion with dependent variables in conservative formulation are discretized. By the use of this formulation, embedded shocks are computed with satisfactory accuracy.

2. A Conservative Formulation of the Equations of Motion

The system of the equations of motion for inviscid three-dimensional flows may be written in conservative or in nonconservative formulation. In [15, 16], a further distinction is made between strong and weak conservative formulations. If we use the nonconservative formulation, the five governing equations (continuity equation, three momentum equations, and energy equation) may be written in a vector–matrix form such as

$$\left[\frac{\partial}{\partial t} + A\frac{\partial}{\partial q_1} + B\frac{\partial}{\partial q_2} + C\frac{\partial}{\partial q_3}\right] X + H = 0, \tag{2.1}$$

where $X^T = (u, v, w, p, \rho)$ is the solution vector, q_i are arbitrary coordinates, H represents curvature terms, and A, B, and C are matrices.

If, for integrating the equations of motion, we use the implicit finite-difference equations employed in [3, 5, 8, 14] and solve these by means of the progonka process, the system of partial differential equations must be written in the form of Eq. (2.1) or

an equivalent vector–matrix form. This means that the differential operators are all applied to the same solution vector (X in Eq. (2.1)). The conservative formulation for arbitrary curvilinear coordinates q_i,

$$\frac{\partial U}{\partial t} + \frac{\partial E}{\partial q_1} + \frac{\partial F}{\partial q_2} + \frac{\partial G}{\partial q_3} + H = 0, \tag{2.2}$$

does not fulfill this condition. In Eq. (2.2), U, E, F, G, and H depend on the selected coordinate system and on the desired formulation of the velocity components.

The system of equations (2.2) can be transformed as follows,

$$\frac{\partial U}{\partial t} + J(U)\frac{\partial U}{\partial q_1} + K(U)\frac{\partial U}{\partial q_2} + L(U)\frac{\partial U}{\partial q_3} + H(U) = 0, \tag{2.3}$$

where $J(U)$, $K(U)$, and $L(U)$ are Jacobi matrices with the element J_{lm}, e.g., given by

$$J_{lm} = \partial E_l / \partial U_m . \tag{2.4}$$

The formulation of the equations of motion (2.3) now fulfills two requirements:

1. The dependent variables are conservative;

2. The differential operators are all applied to the same solution vector U (necessary provision for the application of the progonka process).

The conservative system

$$\frac{\partial U}{\partial t} + \frac{\partial (J(U)\, U)}{\partial q_1} + \frac{\partial (K(U)\, U)}{\partial q_2} + \frac{\partial (L(U)\, U)}{\partial q_3} + H(U) = 0, \tag{2.5}$$

coincides with the equation system (2.3) [27], as is demonstrated by means of an example.

2.1. *Remarks on the Conservative Formulation of the Equations of Motion*

The one-dimensional nonstationary Eulerian equations are considered. In nonconservative form with the dependent variables, u, p and ρ, these read

$$\left[\frac{\partial}{\partial t} + A\frac{\partial}{\partial x}\right] X = 0; \qquad A = \begin{pmatrix} u & \rho^{-1} & 0 \\ c^2\rho & u & 0 \\ \rho & 0 & u \end{pmatrix}; \qquad X = \begin{pmatrix} u \\ p \\ \rho \end{pmatrix}. \tag{2.6}$$

The conservative formulation yields

$$\frac{\partial U}{\partial t} + \frac{\partial E(U)}{\partial x} = 0; \quad E(U) = \begin{pmatrix} m \\ \dfrac{m^2}{\rho} + p \\ (e + p)\dfrac{m}{\rho} \end{pmatrix}; \quad U = \begin{pmatrix} \rho \\ m = \rho u \\ e = \dfrac{p}{\gamma - 1} + \dfrac{m^2}{2\rho} \end{pmatrix}. \tag{2.7}$$

Using the homogeneity relation according to Euler [28] there is also

$$J(U) = \begin{pmatrix} 0 & 1 & 0 \\ \frac{-(3-\gamma)\,m^2}{2\rho^2} & (3-\gamma)\,\frac{m}{\rho} & (\gamma-1) \\ -\gamma\,\frac{me}{\rho^2} + (\gamma-1)\,\frac{m^3}{\rho^3} & \frac{\gamma e}{\rho} - \frac{3(\gamma-1)}{2}\,\frac{m^2}{\rho^2} & \gamma\,\frac{m}{\rho} \end{pmatrix};$$

$$\frac{\partial U}{\partial t} + J(U)\,\frac{\partial U}{\partial x} = 0 \tag{2.8}$$

$$\frac{\partial U}{\partial t} + \frac{\partial (J(U)\,U)}{\partial x} = 0 \tag{2.9}$$

If we regard, for instance, the momentum equations from Eqs. (2.7), (2.8), and (2.9),

$$\frac{\partial m}{\partial t} + \frac{\partial}{\partial x}\left((\gamma-1)\,e + \frac{(3-\gamma)}{2}\,\frac{m^2}{\rho}\right) = 0, \tag{2.7i}$$

$$\frac{\partial m}{\partial t} - \frac{(3-\gamma)}{2}\,\frac{m^2}{\rho^2}\,\frac{\partial \rho}{\partial x} + (3-\gamma)\,\frac{m}{\rho}\,\frac{\partial m}{\partial x} + (\gamma-1)\,\frac{\partial e}{\partial x} = 0, \tag{2.8i}$$

$$\frac{\partial m}{\partial t} + \frac{\partial}{\partial x}\left(-\frac{(3-\gamma)}{2}\,\frac{m^2}{\rho^2}\,\rho + (3-\gamma)\,\frac{m}{\rho}\,m + (\gamma-1)\,e\right) = 0, \tag{2.9i}$$

we see that Eq. (2.7i) and Eq. (2.9i) are indeed identical. Hence we can conjecture that the character of Eq. (2.8) and/or Eq. (2.8i) is also almost conservative, since $(\partial J(U)/\partial x)U = 0$. By the use of an example, which has already been calculated by Lax [19] with Eq. (2.7), it is shown that the calculation of discontinuities with Eq. (2.8) supplies results of at least the same quality as with Eq. (2.7) (see Figs. 1 and 2).

The nonconservative formulation, Eq. (2.6), however, represents the location and intensity of the shock in a distorted way. According to Lax, the time derivatives are replaced by the forward difference

$$\left(\frac{\partial f}{\partial t}\right)_k^n \to \frac{f_k^{n+1} - \overline{f_k^n}}{\Delta t} + O(\Delta t)$$

with

$$\overline{f_k^n} = \tfrac{1}{2}(f_{k+1}^n + f_{k-1}^n),$$

while the derivatives in the x-direction are approximated by the central difference

$$\left(\frac{\partial f}{\partial x}\right)_k^n \to \frac{f_{k+1}^n - f_{k-1}^n}{2\Delta x} + O(\Delta x)^2.$$

This example has for $t = 0$ the initial data $p_l = 50$, $\rho_l = 50$, $u_l = 2$ for $x < 0$ and $p_r = 0$, $\rho_r = 10$, $u_r = 0$ for $x > 0$ with $\gamma = 1.5$ and $\Delta t/\Delta x = 0.25$. After $n = 49$ (Fig. 1) and $n = 99$ (Fig. 2) time steps the density characteristics calculated with Eq. (2.8) are closer to the exact solution than those of Eq. (2.7). The plots of the density functions in Fig. 1 ($n = 49$) have been smoothed after finishing the calculation.

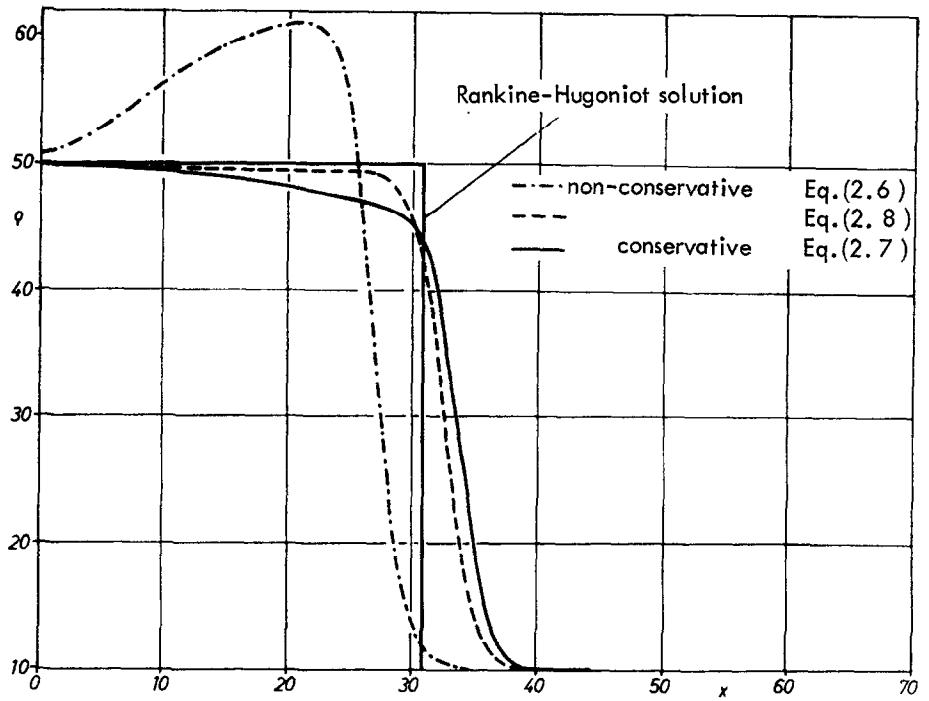

FIG. 1. Comparisons between the shock solutions of three different formulations for the Eulerian equations; $n = 49$; Lax algorithm.

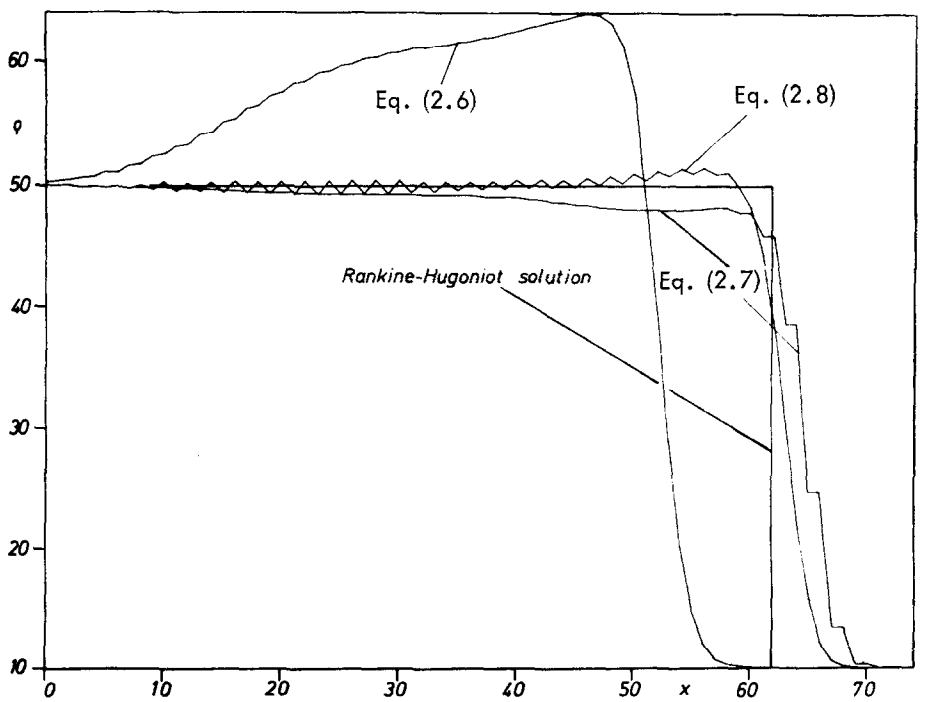

FIG. 2. Comparisons between the shock solutions of three different formulations for the Eulerian equations; $n = 99$; Lax algorithm.

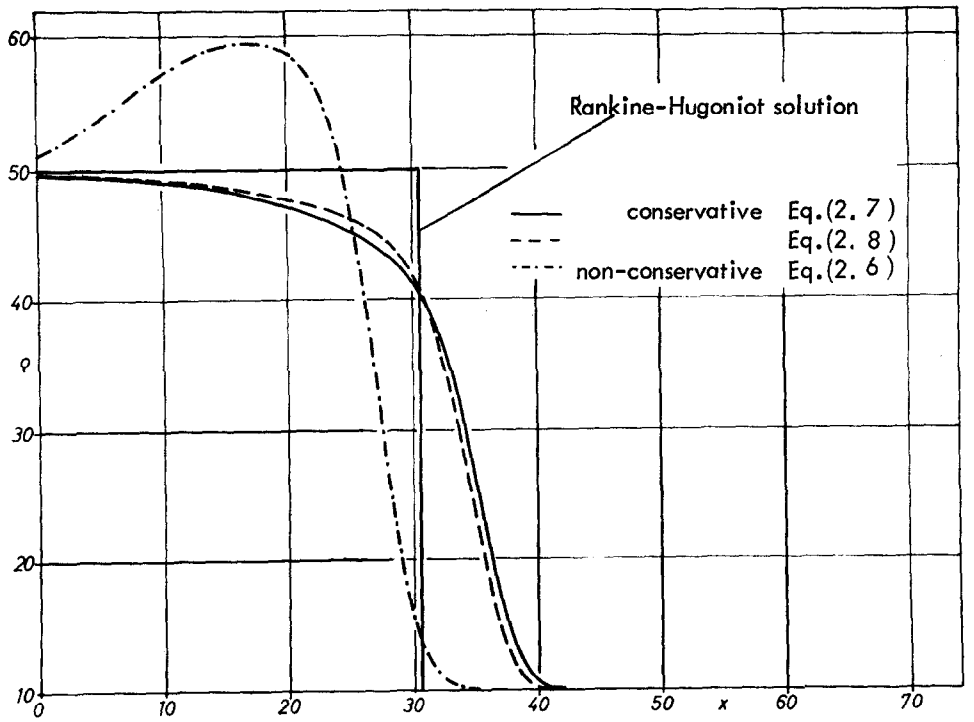

FIG. 3. Comparisons between the shock solutions of three different formulations for the Eulerian equations; $n = 49$; Crank–Nicholson algorithm.

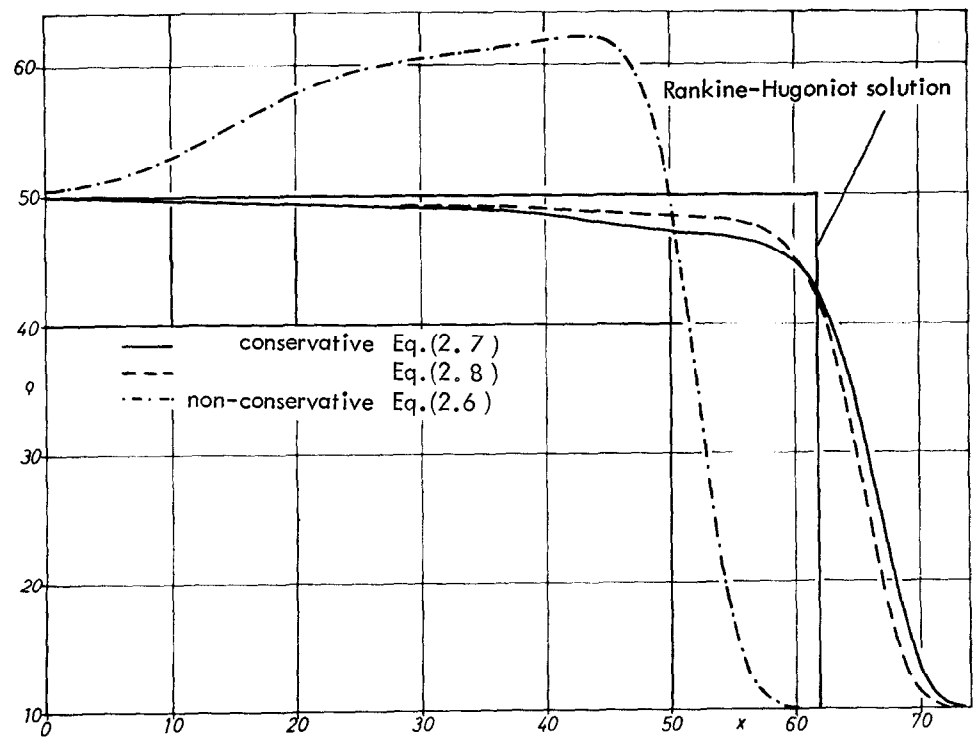

FIG. 4. Comparisons between the shock solutions of three different formulations for the Eulerian equations; $n = 99$; Crank–Nicholson algorithm.

Figure 2 shows the nonsmoothed plots for $n = 99$. The same result from a qualitative point of view is reached with the implicit difference scheme of Crank–Nicholson (Figs. 3 and 4). Here both the temporal and the spatial derivatives are substituted by central differences,

$$\left(\frac{\partial f}{\partial t}\right)_k^{n+1/2} \to \frac{f_k^{n+1} - \overline{f_k}^n}{\Delta t} + O(\Delta t)^2$$

and

$$\left(\frac{\partial f}{\partial x}\right)_k^{n+1/2} \to \frac{f_{k+1}^{n+1} - f_{k-1}^{n+1} + f_{k+1}^n - f_{k-1}^n}{4\Delta x} + O(\Delta x)^2.$$

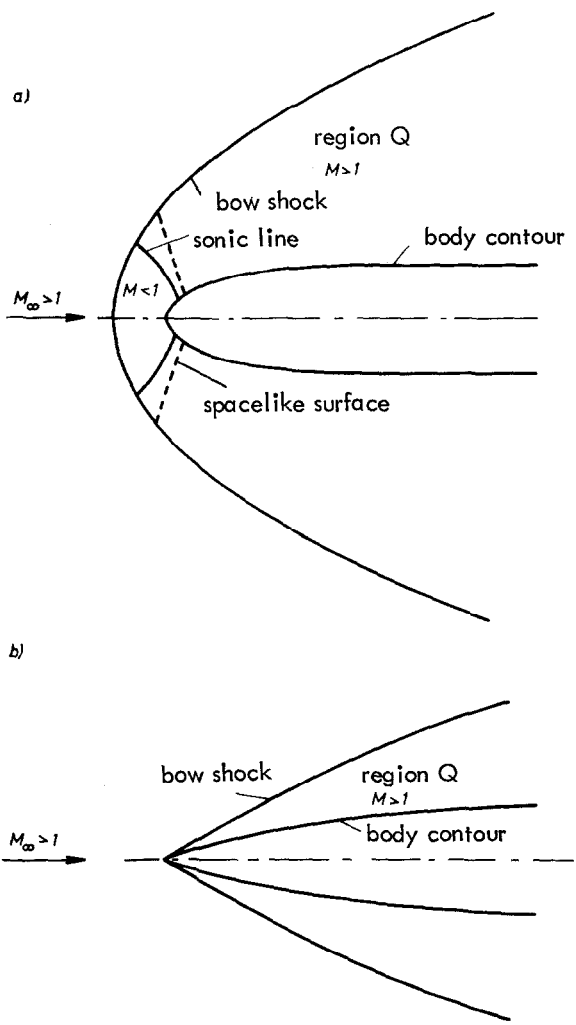

FIG. 5. The areas of calculation in the cases of (a) blunt body and (b) pointed body.

Since the difference equations are solved iteratively, the density function in the region of the shock is smeared to a greater extent than displayed in Figs. 1 and 2. No further smoothing was necessary.

From these and other calculations serving as examples, the conclusion is drawn that calculation of shock waves embedded in the flow field with the equation system in vector–matrix form, where the dependent variables are in conservative formulation, Eq. (2.3), gives at least the same degree of accuracy as calculations by means of the system of equations in divergence form, Eq. (2.2).

2.2. *A Complete Representation of the Equations for Three-Dimensional Flow Fields*

In the present paper, the three-dimensional stationary purely supersonic flow field which occurs in the regions Q is calculated at bodies (Fig. 5). Calculation of embedded subsonic fields, as they arise in the stagnation zone of a blunt body or behind embedded strong shock waves, can be performed with the difference methods [3, 5, 7, 12] (initial procedure). These are based on the nonstationary three-dimensional Eulerian equations, and in the case of stationary boundary conditions the time asymptotes are considered as the desired solutions.

In cylindrical coordinates z, r and φ the stationary equation system (2.3) has the form

$$\left[J(U)\frac{\partial}{\partial z} + K(U)\frac{\partial}{\partial r} + L(U)\frac{\partial}{\partial \varphi}\right] U + H(U) = 0. \tag{2.10}$$

(The use of the cylindrical coordinates does not imply that the body must necessarily be a body of revolution.)

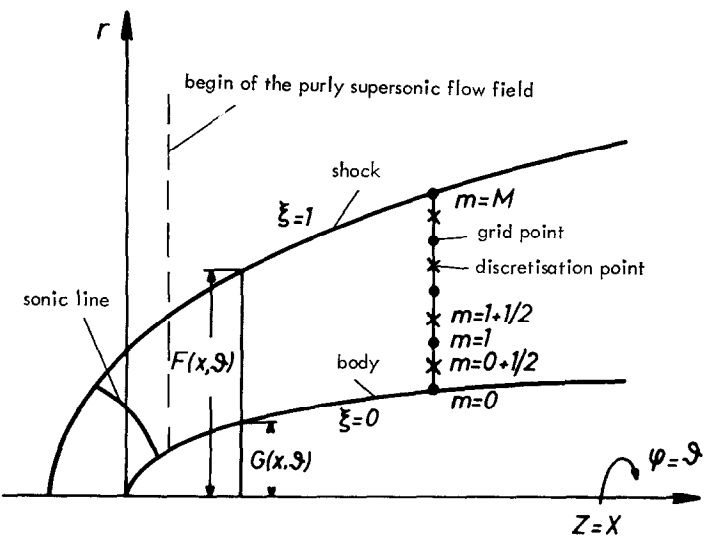

FIG. 6. The coordinate system x, ξ, ϑ; location of grid and discretisation points along a ray.

$$J(U) = \left\| \begin{array}{c|c|c|c} 0 & 1 & 0 & 0 \\ \frac{1}{2\rho^2}[(\gamma-1)m^2 - 2m_1^2] & -(\gamma-3)\frac{m_1}{\rho} & -(\gamma-1)\frac{m_3}{\rho} & (\gamma-1) \\ -\frac{m_1 m_2}{\rho^2} & \frac{m_2}{\rho} & 0 & 0 \\ -\frac{m_1 m_3}{\rho^2} & \frac{m_3}{\rho} & \frac{m_1}{\rho} & 0 \\ m_1 k & \gamma\frac{e}{\rho} - \frac{(\gamma-1)}{2\rho^2}(m^2 + 2m_1^2) & -(\gamma-1)\frac{m_1 m_3}{\rho^2} & \frac{m_1}{\rho}\gamma \end{array} \right\|,$$

$$K(U) = \left\| \begin{array}{c|c|c|c} 0 & 0 & 1 & 0 \\ -\frac{m_2 m_1}{\rho^2} & \frac{m_2}{\rho} & \frac{m_1}{\rho} & 0 \\ \frac{1}{2\rho^2}[(\gamma-1)m^2 - 2m_2^2] & -(\gamma-1)\frac{m_1}{\rho} & -(\gamma-3)\frac{m_2}{\rho} & (\gamma-1) \\ -\frac{m_2 m_3}{\rho^2} & 0 & \frac{m_3}{\rho} & 0 \\ m_2 k & -(\gamma-1)\frac{m_2 m_1}{\rho^2} & \gamma\frac{e}{\rho} - \frac{(\gamma-1)}{2\rho^2}(m^2 + 2m_2^2) & \frac{m_2}{\rho}\gamma \end{array} \right\|, \tag{2.11}$$

$$L(U) = \frac{1}{r}\left[\begin{array}{c|c|c|c} 0 & 0 & 0 & 0 \\ \frac{m_3 m_1}{\rho^2} & \frac{m_3}{\rho} & 0 & 0 \\ \frac{m_3 m_2}{\rho^2} & 0 & 0 & 0 \\ \frac{1}{2\rho^2}\left[(\gamma-1)m^2 - 2m_3^2\right] & -(\gamma-1)\frac{m_1}{\rho} & -(\gamma-3)\frac{m_3}{\rho} & (\gamma-1) \\ m_3 k & -(\gamma-1)\frac{m_3 m_1}{\rho^2} & -(\gamma-1)\frac{m_3 m_2}{\rho^2} & \frac{m_3}{\rho}\gamma \end{array}\right],$$

$$H(U) = \frac{1}{r}\begin{bmatrix} m_2 \\ \frac{m_2 m_1}{\rho} \\ \frac{m_2^2 - m_3^2}{\rho} \\ \frac{2m_2 m_3}{\rho} \\ (e+p)\frac{m_2}{\rho} \end{bmatrix}$$

$$m^2 = |\,\mathbf{m}\,|^2 = m_1^2 + m_2^2 + m_3^2,$$
$$k = \left[-\gamma e + \frac{(\gamma-1)m^2}{\rho}\right]\Big/\rho^2,$$
$$\mathbf{m} = \rho(u i_z + v i_r + w i_\varphi),$$
i_z, i_r, i_φ, are the basis vectors of the cylindrical coordinate system.

(2.11)

(*Continued*)

2.3. *Coordinate System*

In more recent papers [3–12, 14, 24, 25], shock and body contours are transformed in such a way that they can be represented by smooth plane surfaces (Fig. 6) which bound the computational domain generated by the transformation

$$\begin{aligned} z &= x, \\ r &= G(x, \vartheta) + \xi^n(F(x, \vartheta) - G(x, \vartheta)), \\ \varphi &= \vartheta. \end{aligned} \tag{2.12}$$

The function $\xi(z, r, \varphi)$ must fulfill the condition $\xi = 0$ on the body and $\xi = 1$ on the shock. The exponent n can be regarded as the regulation factor for the point density

in the computational network. If $n > 1$, the grid points near the body increase in density, while for $n < 1$ the point density in the vicinity of the bow shock becomes larger. Transformation of the system of equations (2.10) to the new calculation coordinates requires that the coordinate derivatives ξ_z, ξ_r, and ξ_φ be known. By means of the Jacobian $\tilde{\Delta} = \partial(z, r, \varphi)/\partial(x, \xi, \vartheta)$ and the relation $\tilde{\Delta}^{-1} = \partial(x, \xi, \vartheta)/\partial(z, r, \varphi)$ we obtain, unless $\tilde{\Delta}$ becomes singular,

$$\xi_z = -r_x/r_\xi\,; \qquad \xi_r = 1/r_\xi\,; \qquad \xi_\varphi = -r_\vartheta/r_\xi\,; \qquad r_\xi = n\xi^{n-1}(F - G). \tag{2.13}$$

Remark: At the position $\xi = 0$, $\tilde{\Delta}$ becomes singular for $n \neq 1$. For $n > 1$, $\tilde{\Delta} = r_\xi = 0$. This means that an infinitesimal volume element in the z, r, φ-coordinate system collapses into a single point in the x, ξ, ϑ-system. Nevertheless, in every small neighborhood of $\xi = 0$ the mapping is unique. $\tilde{\Delta} = r_\xi$ appears in the transformations (2.13) as a factor. These transformations are employed only at $\xi = 0$ in Eq. (2.14), but this formula reduces to

$$\mathbf{v} \cdot \mathbf{n} = \frac{u\xi_z + v\xi_r + (1/r)\, w\xi_\varphi}{[\xi_z^{\,2} + \xi_r^{\,2} + (1/r^2)\, \xi_\varphi^{\,2}]^{1/2}} = \frac{-ur_x + v - (1/r)\, wr_\vartheta}{[r_x^{\,2} + 1 + (1/r^2)\, r_\vartheta^{\,2}]^{1/2}} = 0$$

since the factor r_ξ cancels out.

2.4. *Boundary Conditions*

The sole requirement on the body is its impermeability for the gas

$$\mathbf{v} \cdot \mathbf{n} = 0, \tag{2.14}$$

where $\mathbf{n} \triangleq$ normal vector of the body surface. The boundary conditions on the shock are given by the generalized Rankine–Hugoniot equations

$$\begin{aligned} \rho v_\lambda &= \rho_\infty v_{\lambda\infty}\,, \qquad v_\lambda = \mathbf{v} \cdot \boldsymbol{\lambda}, \\ p + \rho_\infty v_{\lambda\infty} v_\lambda &= p_\infty + \rho_\infty v_{\lambda\infty}^2\,, \\ h + v_\lambda^2/2 &= h_\infty + v_{\lambda\infty}^2/2, \\ \mathbf{v} \times \boldsymbol{\lambda} &= \mathbf{v}_\infty \times \boldsymbol{\lambda}. \end{aligned} \tag{2.15}$$

The index ∞ denotes the freestream quantities, $\boldsymbol{\lambda} \triangleq$ normal vector of the bow shock contour.

The last equation of Eqs. (2.15) is a vector equation with two linearly independent components which express the conservation of the velocity component in the tangential plane of the shock.

2.5. *Transformed System of Equation*

In the coordinates (x, ξ, ϑ), the system of equation (2.10) assumes the form

$$\left[J(U)\frac{\partial}{\partial x} + \overline{K(U)}\frac{\partial}{\partial \xi} + L(U)\frac{\partial}{\partial \vartheta}\right] U + H(U) = 0 \tag{2.16}$$

with

$$\overline{K(U)} = J(U)\,\xi_z + K(U)\,\xi_r + L(U)\,\xi_\varphi .$$

The boundary conditions are formulated in the dependent variables ρ, $\mathbf{m}$, e. Hence on the body we obtain from Eq. (2.14)

$$m_1\xi_z + m_2\xi_r + m_3(1/r)\,\xi_\varphi = 0. \tag{2.17}$$

Here the fact was used that the coordinate surface $\xi = 0$ just represents the body contour and thus the body normal is given by

$$\mathbf{n}^T = \frac{\xi_z\,,\ \xi_r\,,\ (1/r)\,\xi_\varphi}{[\xi_z{}^2 + \xi_r{}^2 + (1/r^2)\,\xi_\varphi{}^2]^{1/2}}\Bigg|_{\xi=0}.$$

Since the bow shock, too, is a coordinate surface $\xi = 1$, the boundary conditions (2.15) can be written as a function of this coordinate.

$$\begin{aligned}
m_1\xi_z + m_2\xi_r + m_3\frac{1}{r}\,\xi_\varphi &= m_{1;\infty}\xi_z + m_{2;\infty}\xi_r + m_{3;\infty}\frac{1}{r}\,\xi_\varphi = \alpha_\infty\,,\\
(\gamma-1)\left(e - e_\infty - \frac{1}{2}\left(\frac{m^2}{\rho} - \frac{m_\infty{}^2}{\rho_\infty}\right)\right) &= \frac{\alpha_\infty{}^2}{\beta^2}\left(\frac{1}{\rho_\infty} - \frac{1}{\rho}\right),\\
\gamma\left(\frac{e}{\rho} - \frac{e_\infty}{\rho_\infty} - \frac{1}{2}\left(\frac{m^2}{\rho^2} - \frac{m_\infty{}^2}{\rho_\infty{}^2}\right)\right) &= \frac{1}{2}\frac{\alpha_\infty{}^2}{\beta^2}\left(\frac{1}{\rho_\infty{}^2} - \frac{1}{\rho^2}\right),\\
\frac{1}{\rho}\left(m_2\frac{1}{r}\,\xi_\varphi - m_3\xi_r\right) &= \frac{1}{\rho_\infty}\left(m_{2;\infty}\frac{1}{r}\,\xi_\varphi - m_{3;\infty}\xi_r\right),\\
\frac{1}{\rho}\,(m_1\xi_r - m_2\xi_z) &= \frac{1}{\rho_\infty}\,(m_{1;\infty}\xi_r - m_{2;\infty}\xi_z),
\end{aligned} \tag{2.18}$$

where $h = (\gamma p/(\gamma-1)\rho)$, $\beta = [\xi_z{}^2 + \xi_r{}^2 + (1/r^2)\,\xi_\varphi{}^2]^{1/2}$. In the system of equations (2.18), apart from the conservative variables ρ, $\mathbf{m}$, and e, the coordinate derivatives ξ_z, ξ_r, and ξ_φ are unknown, too. Equations (2.12) and (2.13) show that at a given body contour an additional variable—the function of the shock contour F—occurs. The missing equation is supplied by the solution method (progonka process) described in [3, 5, 8, 14].

3. Finite-Difference Equations

The equation system (2.16) is approximated by the finite-difference equations according to Babenko *et al.* [14, 8]. In the computational domain bounded by flat surfaces, an orthogonal difference mesh with the mesh intervals $\Delta x = \tau$, $\Delta\xi = h_1$, $\Delta\vartheta = h_2$ is

introduced. If M, L indicate the numbers of the mesh intervals in the ξ, ϑ directions, then

$$x^n = \sum_{i=1}^{n} \tau^i + x^0; \qquad \xi_m = mh_1; \qquad \vartheta_l = lh_2; \qquad m = 1 \cdots M, \quad l = 1 \cdots L,$$

$$\kappa_1 = \frac{\tau}{h_1}; \qquad \kappa_2 = \frac{\tau}{h_2}. \tag{3.1}$$

The solution vector at the point x^n, ξ_m, ϑ_l is denoted by $U(x^n, \xi_m, \vartheta_l) \equiv U^n_{m,l}$. For reasons of clear presentation of the difference equations, the transformation operators

$$P_0 U^{n+(j)}_{m,l} = U^{n+(j+1)}_{m,l} \quad \text{or} \quad P_0^{(j+1)} U^n_{m,l} = U^{n+(j+1)}_{m,l},$$

$$P_1 U^n_{m,l} = U^n_{m+1,l}, \qquad P_2 U^n_{m,l} = U^n_{m,l+1},$$

$$I U^n_{m,l} = U^n_{m,l}$$

are introduced. Hence the finite-difference operators, which approximate the differential operators of Eq. (2.16) read as follows [8]:

$$2\tau \left(\frac{\partial}{\partial x}\right)^{n+(j/2)}_{m+1/2,l} \to \Delta_{x,j} = (P_1 + I)\left(P_0{}^j - I - \frac{\sigma_1 \kappa_2}{4}(P_2 - 2I + P_2^{-1})\right),$$

$$h_1 \left(\frac{\partial}{\partial \xi}\right)^{n+(j/2)}_{m+1/2,l} \to \Delta_{\xi,j} = (P_1 - I)(\bar{\alpha} P_0{}^j + \bar{\beta} I), \tag{3.3}$$

$$4h_2 \left(\frac{\partial}{\partial \vartheta}\right)^{n+(j/2)}_{m+1/2,l} \to \Delta_{\vartheta,j} = (P_1 + I)(P_2 - P_2^{-1})(\bar{\alpha} P_0{}^j + \bar{\beta} I).$$

The parameters σ_1, $\bar{\alpha}$, and $\bar{\beta}$ are always positive and it is required that $\bar{\alpha} + \bar{\beta} = 1$. For reasons of stability there must be $\bar{\alpha} > \bar{\beta}$ [5, 14]. If Eq. (3.3) is substituted into Eq. (2.16), we obtain a system of five finite-difference equations

$$[J(U)^{n+(j/2)}_{m+1/2,l} \Delta_{x,j+1} + 2\kappa_1 \overline{K(U)}^{n+(j/2)}_{m+1/2,l} \Delta_{\xi,j+1} + \tfrac{1}{2}\kappa_2 L(U)^{n+(j/2)}_{m+1/2,l} \Delta_{\vartheta,j}]\, U^n_{m,l} + 2\tau H(U)^{n+(j/2)}_{m+1/2,l} = 0. \tag{3.4}$$

From the system of equations (3.4) it is seen that the discretization is performed on intermediate grid points for the ξ-direction, and with averaged iteration steps for the x-(hyperbolic) direction. The iteration in the x-direction (index j) becomes necessary because of the quasi-linearity of the initial equation system and the implicit character of the finite-difference equations. Along a ray (Fig. 6), $m = 0, 1, \ldots, M$, $5M$ equations

condition on the body. These are opposed by $5(M + 1)$ dependent variables and the function F of the bow shock as unknowns sothat along a ray the system of equation is closed.

The solution of the implicit finite-difference equation system (3.4), including the boundary conditions (2.17) and (2.18), requires a particular effort which is accounted for by the application of the progonka process.

4. Solution Method

References [3, 5, 8, 12, 14] describe in great detail the application of the progonka process to the finite-difference approximations of systems of differential equations for three-dimensional stationary or nonstationary formulations with the dependent variables being nonconservative. The progonka process in the form used here can be applied logically only if the domain of calculation is bounded in the ξ-direction by a wall ($\xi = 0$), which can possibly be moved, and by a shock ($\xi = 1$). If, as in this case, the dependent variables are used in conservative formulation, nothing of the principles of the progonka process is changed, but it seems convenient to indicate—because of the enormous algebraic effort—the quantities required for the individual calculation methods.

4.1. *Forward Computation*

The computation starts with the use of Eq. (2.17) for the boundary condition on the body which is written in the form

$$\begin{aligned} &\mu_m U_{m,l}^{n+(j+1)} = g_m, \qquad m = 0 \text{ corresponds to the mesh point of the body,} \\ &\mu_0 = (0, \xi_z, \xi_r, (1/r)\,\xi_\varphi, 0)_{0,l}^{n+(j)}, \qquad g_0 = 0. \end{aligned} \tag{4.1}$$

If the equation system (3.4) is transformed,

$$s_{m+1/2,l}^{n+(j/2)} U_{m+1,l}^{n+(j+1)} + t_{m+1/2,l}^{n+(j/2)} U_{m,l}^{n+(j+1)} = f_{m+1/2,l}^{n+(j/2)}, \tag{4.2}$$

where

$$\begin{aligned} f_{m+1/2,l}^{n+(j/2)} = {} & [J(U)_{m+1/2,l}^{n+(j/2)} (P_1 + I)(I + (\sigma_1\kappa_2/4)(P_2 - 2I + P_2^{-1})) \\ & - 2\bar{\beta}\kappa_1 \overline{K(U)}_{m+1/2,l}^{n+(j/2)} (P_1 - I) - (\kappa_2/2)\, L(U)_{m+1/2,l}^{n+(j/2)} \Delta_{\vartheta,j}]\, U_{m,l}^{n} \\ & - 2\tau H(U)_{m+1/2,l}^{n+(j/2)}, \\ s = {} & J(U) + 2\bar{\alpha}\kappa_1 \overline{K(U)}, \qquad t = J(U) - 2\bar{\alpha}\kappa_1 \overline{K(U)}, \end{aligned}$$

one obtains, by use of Eq. (4.1) for $0 < m \leqslant M$, the recursion coefficients μ_{m+1}, g_{m+1} [8, 14] to (for reasons of clarity the indices n, j, l are omitted)

$$\begin{aligned} \mu_{m+1} &= \frac{\mu_m(\tau s)_{m+1/2}}{\| \mu_m(\tau s)_{m+1/2} \|}, \\ g_{m+1} &= \frac{\mu_m(\tau f)_{m+1/2} - \Delta_{m+1/2} g_m}{\| \mu_m(\tau s)_{m+1/2} \|}, \end{aligned} \tag{4.3}$$

where

$$\tau_{m+1/2} = (t^{-1}\Delta)_{m+1/2}, \qquad \Delta_{m+1/2} = \det | t_{m+1/2} |.$$

To prevent the recursion coefficients (4.3) from growing beyond all measure, they are limited by means of the maximum norm

$$\| \mu_m(\tau s)_{m+1/2} \| = \| \mu_{m+1} \| = \max | \mu_{i;m+1} |, \qquad i = 1,..., 5.$$

Appendix A lists the elements of the matrices $t_{m+1/2}$, $s_{m+1/2}$ as well as those of $\tau_{m+1/2}$ for the equation system used here.

4.2. *Solution of the System of Finite-Difference Equations at the Shock*

On the basis of the values g_0, μ_0 on the body, the values of g_m, μ_m can be calculated on all mesh points along a coordinate line $x = \text{const}$ until the shock. For calculation of the six unknowns on the shock, ρ, $\mathbf{m}$, e, and F, the five Hugoniot equations (2.18), and the equation $\mu_M U_M = g_M$ ($m = M$ corresponds to a mesh point on the $\xi = 1$ line) are available. This system of transcendental equations can now be solved by iteration. Reference [8] provides detailed information on the iteration method used so that in this place only the equations to be iterated are indicated. If the relation

$$g_\infty = \mu_1\rho_\infty + \mu_2 m_{1;\infty} + \mu_3 m_{2;\infty} + \mu_4 m_{3;\infty} + \mu_5 e_\infty$$

is introduced, the system of equations

$$\varphi(\xi_z |_{\xi=1} = -F_{x;l}^{(s+1)}) = \frac{1}{m_{1;\infty}} \left[-m_{2;\infty} - m_{3;\infty} \frac{1}{r} \xi_\varphi + \frac{\beta^2}{\mu_\nu} \left\{ \frac{g_M - g_\infty}{1 - (\rho^{(s)}/\rho_\infty)} + g_\infty - \mu_5 \right.\right.$$
$$\left.\left. \times \left[e_\infty + \frac{\alpha_\infty{}^2}{\rho_\infty \beta^2} \left(\frac{1}{2} \left[\frac{\rho_\infty}{\rho^{(s)}} + 1 \right] - \frac{\rho_\infty}{\rho^{(s)}(\gamma - 1)} \right) - \frac{1}{2} \frac{m_\infty{}^2}{\rho_\infty} \right] \right\} \right],$$
$$\frac{\rho^{(s)}}{\rho_\infty} = \frac{(\gamma + 1)\, \alpha_\infty{}^2}{(\gamma - 1)[\gamma\beta^2(2e_\infty\rho_\infty - m_\infty{}^2) + \alpha_\infty{}^2]} \tag{4.4}$$

(s corresponds to the number of iterations),

$$\mu_\nu = \mu_2\xi_z + \mu_3\xi_r + \mu_4(1/r)\, \xi_\varphi$$

can be used to determine by iteration the derivative of the shock contour function F in the x-direction. α_∞ and β are calculated for $\xi = 1$ according to Eq. (2.18). Furthermore, $\xi_z = -F_x/r_\xi$, $\xi_r = 1/r_\xi$, and $(1/r)\, \xi_\varphi = -F_\vartheta/r_\xi F$. r_ξ may be canceled out of the system (2.18). The expression $(F_\vartheta/F)_l^{n+(j)}$ is approximated by $(1/2h_2F_l^{n+(j)})$ $[F_{l+1}^{n+(j)} - F_{l-1}^{n+(j)}]$. From (4.4) one obtains $F_{x;l}^{(s+1)} \equiv F_{x;l}^{n+(j+1)}$ and $\rho^{(s)} = \rho_M$, from which the remaining unknowns can be calculated:

$$\begin{aligned}
m_{1;M} &= (\rho_M/\rho_\infty)\, m_{1;\infty} + \xi_z \Lambda_M, \\
m_{2;M} &= (\rho_M/\rho_\infty)\, m_{2;\infty} + \xi_r \Lambda_M, \\
m_{3;M} &= (\rho_M/\rho_\infty)\, m_{3;\infty} + (1/r)\, \xi_\varphi \Lambda_M, \\
e_M &= e_\infty + \frac{1}{2} \Lambda_M \left[\frac{\rho_\infty}{\rho_M} \left(\frac{\gamma - 3}{\gamma - 1} + \frac{\rho_M}{\rho_\infty} \right) - \frac{\beta^2 m_\infty{}^2}{\rho_\infty \alpha_\infty} \right], \\
F_l^{n+(j+1)} &= F_l{}^n + \tau(\bar{\alpha} F_{x;l}^{n+(j+1)} + \bar{\beta} F_{x;l}^n), \\
\Lambda_M &= (\alpha_\infty/\beta^2)[1 - \rho_M/\rho_\infty].
\end{aligned} \tag{4.5}$$

4.3. *Backward Computation*

When the dependent variables are determined at $m = M$ (bow shock), then the solution vectors $U_{M-1,l}^{n+(j+1)}$, $U_{M-2,l}^{n+(j+1)}$,..., $U_{0,l}^{n+(j+1)}$ are calculated by the use of the first four components of Eq. (4.2) and Eq. (4.1). Practical computation has shown that during the solution of Eqs. (4.1) and (4.2) undetermined terms of the type 0/0 can appear, depending on angle of attack and body curvature. Appendix B presents a system of equations which avoids these difficulties.

Now the system of equations for calculating the flow variables and the shock contour along a ray is complete. The stability of the finite-difference equations has not been considered. The determination of the step size was done according to the equation given in [8, 14], which is based on a stability analysis of the nonconservative system of equations (2.1).

5. Results

By means of the finite-difference method described above, the flow fields around various body contours have been calculated. Compression zones, embedded shock waves, and expansion zones appear in the flow field as a function of angle of attack, Mach number, and body contour. Some examples of the computation are given. A detailed analysis of a variety of flow fields is given in [29]. Figures 7 and 8a show the fields of characteristics calculated from the solutions for the flows around a blunted

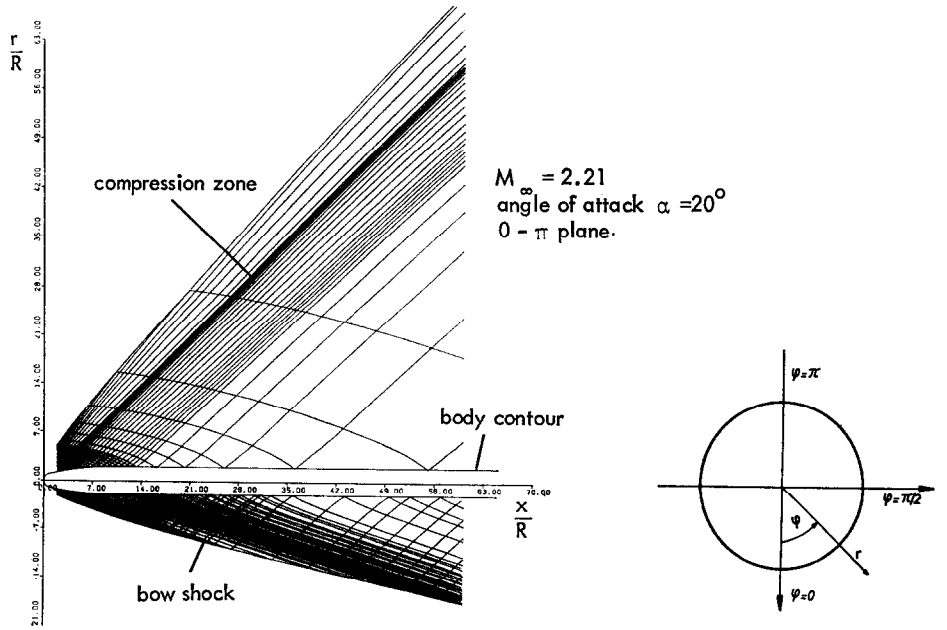

FIG. 7. The characteristics for a flow field around a blunted ogive cylinder.

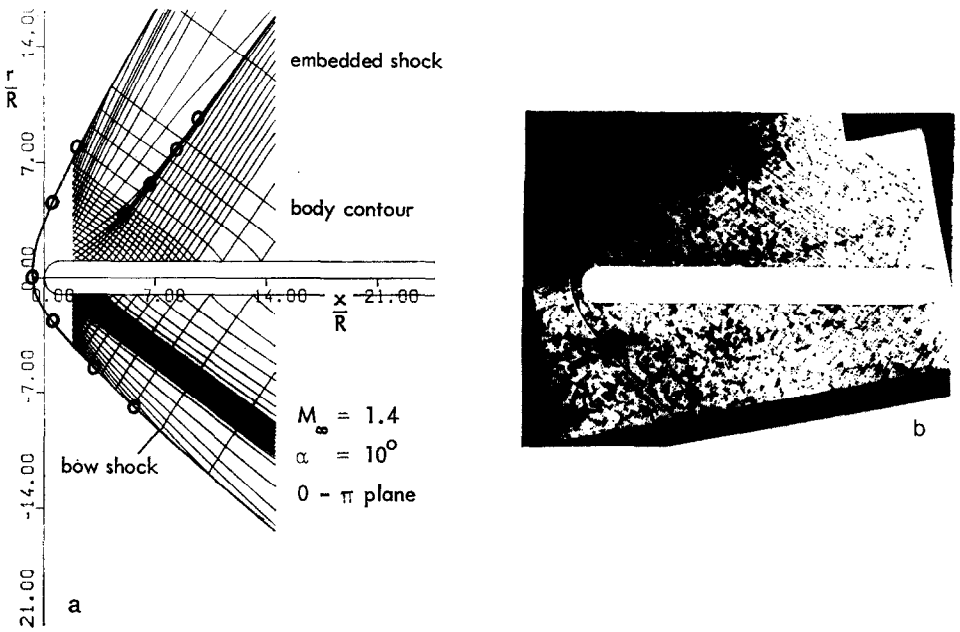

FIG. 8. (a) The characteristics for a flow field around a hemisphere cylinder; ○ Experiment [30]. (b) Schlierenphotograph of the flow around a hemisphere cylinder (after T. Hsieh [30]). $M_\infty = 1.4$, $\alpha = 10°$.

ogive cylinder and a hemisphere cylinder. The Mach numbers are $M_\infty = 2.21$ and $M_\infty = 1.4$, the angles of attack are $\alpha = 20°$ and $\alpha = 10°$. The lengths indicated are normalized with the radius of the spherical nose. In Fig. 7 compression zones can be seen on the leeward side which occur because of the curvature jump at the junction between sphere and ogive (very marked) and at the ogive cylinder junction. A similar phenomenon occurs on the windward side; however, this is only visible in the real part of the field due to the extraordinary density of the characteristics and their reflection at the bow shock. After a short distance, the bow shock on the leeward side changes over to a Mach line (the shock intensity goes towards zero). In Fig. 8a, an embedded shock can be seen on the leeward side. The predicted contours of the bow shock and the embedded shock are compared with the experimental data of Hsieh [30] (Fig. 8b). The agreement is very satisfactory even for these low supersonic freestream Mach numbers. Static pressure measurements at a pointed ogive cylinder are given in [31]. Since, as is known, the nose form of a body has only a minor effect on the static pressure downstream of this nose, the experimental data [31] can be compared with those calculated on the spherically blunted ogive cylinder described above. Figures 9 and 10 show the comparison for $M_\infty = 1.46$ and angles of attack $\alpha = 5°$, 10°. Both in the experiment and in theory the static pressure changes (Fig. 9) which occur because of reflection of the compression waves on the body surface are observed. Figure 10 contains also the results of a calculation done by v.d. Vyle [32] with the aid of Kutler's procedure [25]. The pressure coefficient diverges from the

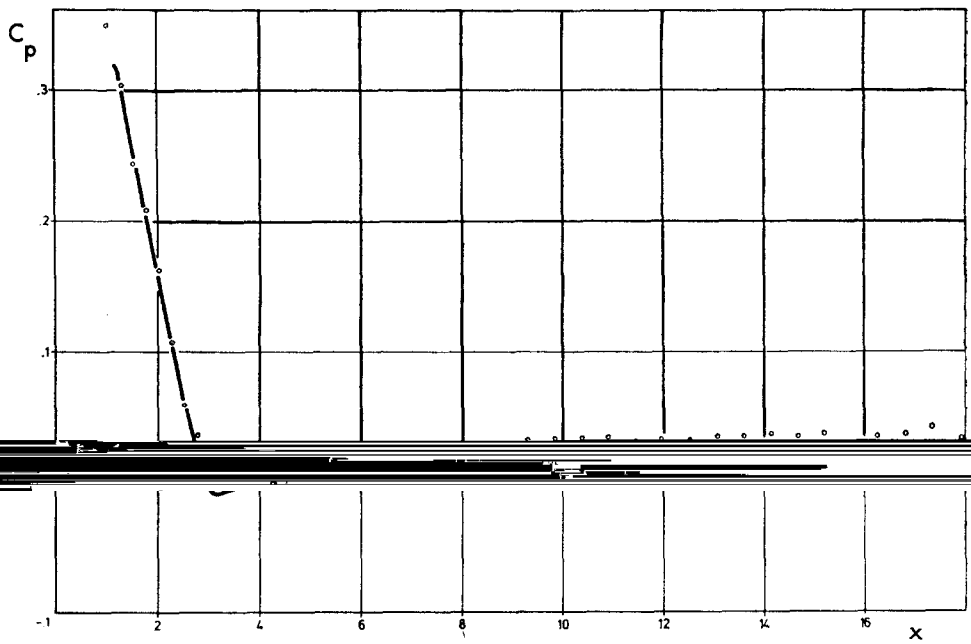

FIG. 9. Pressure distribution along the body surface, windward side ($\varphi = 0°$). $M_\infty = 1.46$, angle of attack $\alpha = 10°$; ○, Experiment, $\mathrm{Re}_D = 0.29 \times 10^6$ [31]; ——, Present theory.

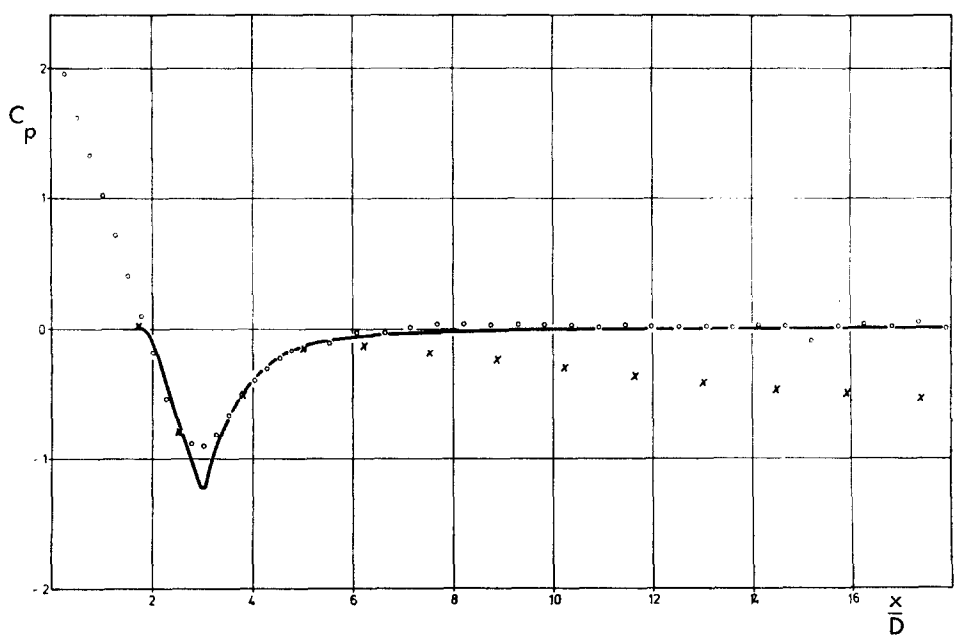

FIG. 10. Pressure distribution along the body surface, leeward side ($\varphi = \pi$). $M_\infty = 1.46$, angle of attack $\alpha = 5°$; ○, Experiment, $\mathrm{Re}_D = 0.29 \times 10^6$ [31]; ——, Present theory; × Theory [32].

experimental data at the rear part of the body, apparently because of the enforcement of constant entropy. With this assumption, ignored, better results have been obtained [32]. The point $x/D = 0$ (Figs. 9 and 10) is in the tip of the ogive cylinder in the experiment [8, 31] (D is the diameter of the cylinder). At greater angles of attack ($\alpha \leqslant 10°$) and appropriately large Mach numbers, embedded shock waves arise in the flow around the abovementioned body, because of crossflow.

The crossflow Mach number M_Q is defined by

$$M_Q = (v^2 + w^2)/c.$$

Here v and w are the components of the velocity vector in the r- and φ-directions. The crossflow Mach number M_Q is not only a function of the variables r, φ but also a function of the variable $z = x$. For every plane $x/D = \text{const}$ another plot was obtained for the lines of constant crossflow Mach number. If the lines of constant crossflow Mach number M_Q are plotted in planes $x/R = \text{const}$ (R = radius of the spherical nose), the generation of a local supersonic field which ends with a shock wave of the crossflow due to the expansion over the cylinder can be clearly seen. Figures 11 and 12 show this behavior for $M_\infty = 2.21$ and $\alpha = 20°$ in the plane $x/R = 18.5$ Figure 12 shows

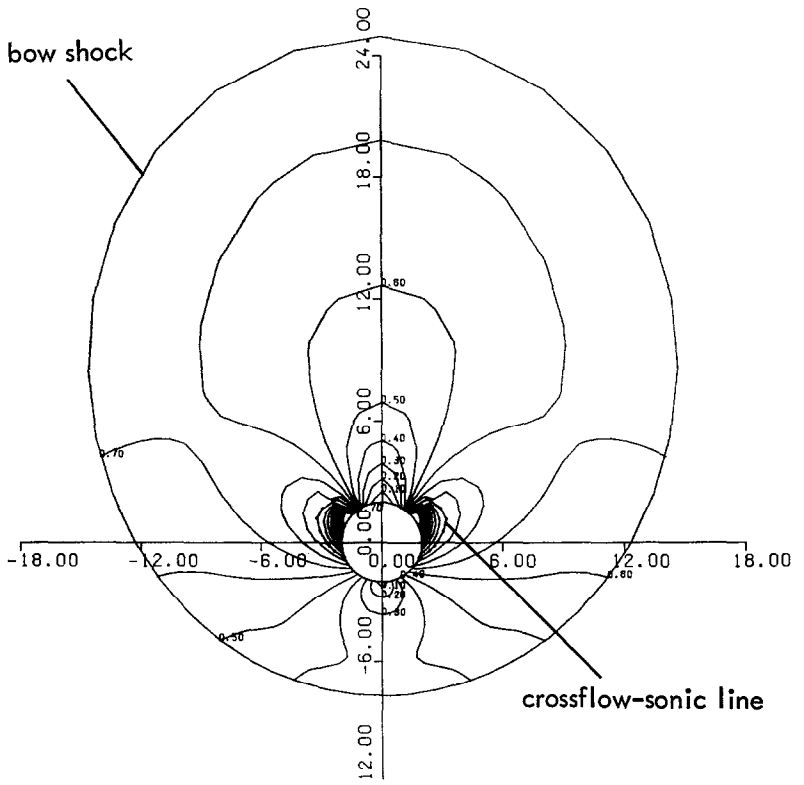

FIG. 11. Lines of constant crossflow Mach number M_Q in the plane $x/R = 18.55$. $M_\infty = 2.21$, $\alpha = 20°$.

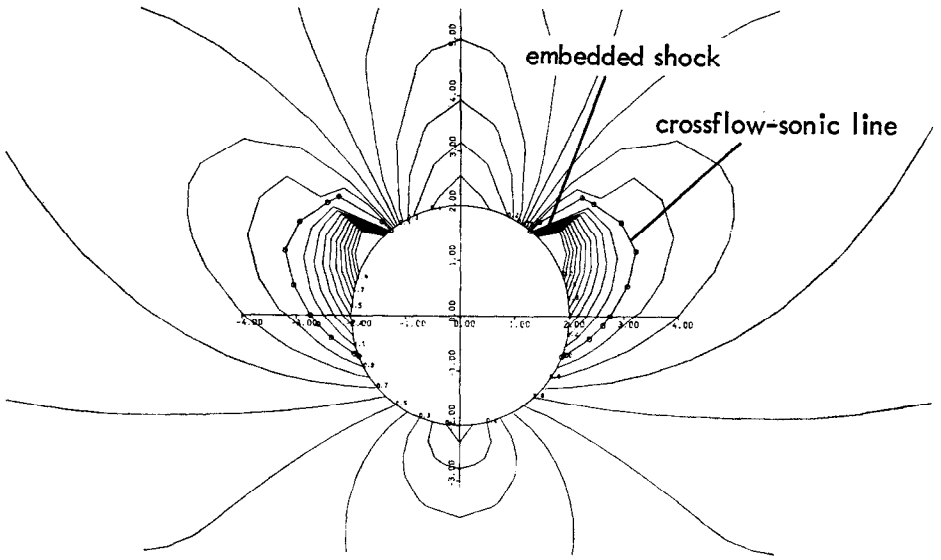

FIG. 12. Lines of constant crossflow Mach number M_Q in the vicinity of the body, enlarged. Plane $x/R = 18.55$; $M_\infty = 2.21$, $\alpha = 20°$.

the enlarged area in the vicinity of the cylinder, with the crossflow supersonic region limited by the sonic line marked with circles. The maximum value of M_Q is approximately 2.5.

If the body contour is changed by a diameter increase (cf. Fig. 13), an embedded shock wave arises at $x/R = 18$ and an expansion zone at $x/R = 20$ due to the discontinuous derivative of body contour function. Figure 13 shows for $M_\infty = 3$, $\alpha = 0°$ the field of characteristics in the region of interest. The location of the embedded shock wave can be seen very distinctly. Figure 14 shows the contour of the bow shock and the characteristics for the flow around a blunted circular cone ($M_\infty = 2.97$, $\alpha = 0°$). Where the sphere changes into the cone, the first derivative of the contour function $G(x, \vartheta)$ is discontinuous. The characteristics plotted on the basis of the difference solution show at the shoulder the expansion fan as expected according to theory. For all sample calculations a grid of $M = 17$ points in the ξ-direction and $L = 19$ points in the ϑ-direction has been used. It has already been mentioned that the step size $\Delta x = \tau$ has been calculated by the equation given in [14, p. 31]. Because the step size τ is a function of the flow variables u, w, c and the coordinate r (for fixed α, β, σ_1, J), one obtains variable τ-values along the x-coordinate. In connection with the calculation of the flow field around a blunted ogive cylinder with $M_\infty = 2.21$ and $\alpha = 20°$ (Figs. 7, 11, and 12) an averaged step size of

$$\bar{\tau} \cong 0.1387$$

was obtained. For the case $M_\infty = 1.46$, $\alpha = 10°$ (Fig. 9) it was

$$\bar{\tau} \cong 0.1622.$$

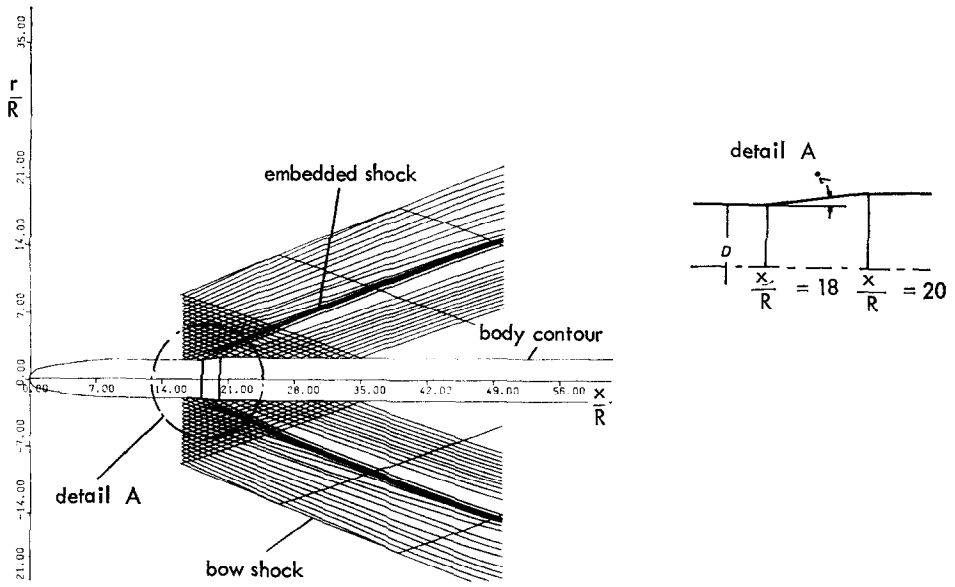

FIG. 13. Flow field around a blunted ogive-cylinder with a 7° shoulder. Characteristics in the area of embedded shock. $M_\infty = 3$, $\alpha = 0°$, 0–π-plane.

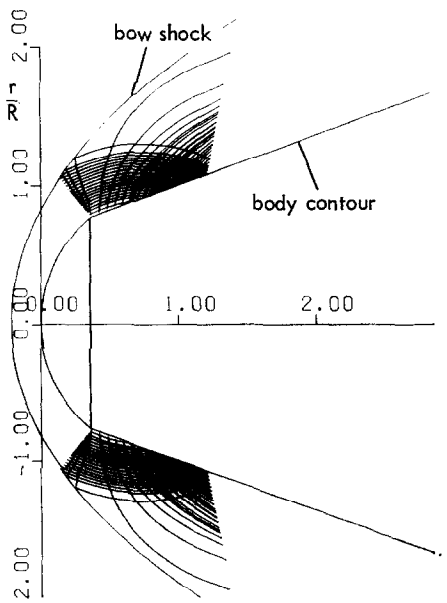

FIG. 14. Flow field around a blunted circular cone with a sharp shoulder. Characteristics in the expansion zone at the shoulder. $M_\infty = 2.97$, $\alpha = 0°$.

6. Concluding Remarks

This paper gives a finite-difference method for calculating three-dimensional inviscid supersonic flow fields. The dependent variables of equations of motion are used in conservative form. In this way it is possible to calculate embedded shock waves with at least the same accuracy as one would get using the equations of motion written in divergence form. The essential advantage of the system of equations used in this paper lies in the application of the progonka process, by means of which field and boundary points can be calculated with the same accuracy. The capability of the method, especially as far as the treatment of embedded shocks is concerned, is proved with the aid of some selected examples. The computations of the flow fields described in this paper (with the exception of subsonic fields in the stagnation areas) required a computing time of 15 to 30 min on a Telefunken TR-440 computer (the CDC 6600 is about four times faster).

Appendix A

The matrices $s_{m+1/2}$ and $t_{m+1/2}$ have the following elements:

$$t_{m+1/2} = \left(\begin{array}{c|c|c|c|c} 0 & \xi_1 & \xi_2 & \xi_3 & 0 \\ \eta\xi_1 - a_1\vartheta & a_1\xi_1 - \delta_1 a_1\xi_1 + \vartheta & a_1\xi_2 - \delta_1 a_2\xi_1 & a_1\xi_3 - \delta_1 a_3\xi_1 & \delta_1\xi_1 \\ \eta\xi_2 - a_2\vartheta & a_2\xi_1 - \delta_1 a_1\xi_2 & a_2\xi_2 - \delta_1 a_2\xi_2 + \vartheta & a_2\xi_3 - \delta_1 a_3\xi_2 & \delta_2\xi_2 \\ \eta\xi_3 - a_3\vartheta & a_3\xi_1 - \delta_1 a_1\xi_3 & a_3\xi_2 - \delta_1 a_2\xi_3 & a_3\xi_3 - \delta_1 a_3\xi_3 + \vartheta & \delta_3\xi_3 \\ \omega\vartheta & (\omega - \eta)\,\xi_1 - \delta_1 a_1\vartheta & (\omega - \eta)\,\xi_2 - \delta_1 a_2\vartheta & (\omega - \eta)\,\xi_3 - \delta_1 a_3\vartheta & \gamma\vartheta \end{array}\right), \tag{A1}$$

$$s_{m+1/2} = \left(\begin{array}{c|c|c|c|c} 0 & -t_{12} & -t_{13} & -t_{14} & 0 \\ 2(\eta - a_1^2) - t_{21} & -2\delta_3 a_1 - t_{22} & -2\delta_1 a_2 - t_{23} & -2\delta_1 a_3 - t_{24} & 2\delta_1 - t_{25} \\ -2a_2 a_1 - t_{31} & 2a_2 - t_{32} & 2a_1 - t_{33} & -t_{34} & -t_{35} \\ -2a_3 a_1 - t_{41} & 2a_3 - t_{42} & -t_{43} & 2a_1 - t_{44} & -t_{45} \\ 2\omega a_1 - t_{51} & -2(\omega - \eta + \delta_1 a_1^2) - t_{52} & -2\delta_1 a_2 a_1 - t_{53} & -2\delta_1 a_3 a_1 - t_{54} & 2\gamma a_1 - t_{55} \end{array}\right).$$

The following abbreviations were used:

$$\mathbf{a} = \begin{pmatrix} a_1 \\ a_2 \\ a_3 \end{pmatrix} = \begin{pmatrix} m_1/\rho \\ m_2/\rho \\ m_3/\rho \end{pmatrix}, \qquad \xi = \begin{pmatrix} \xi_1 \\ \xi_2 \\ \xi_3 \end{pmatrix} = \begin{pmatrix} 1 - 2\bar{\alpha}\kappa_1\xi_z \\ -2\bar{\alpha}\kappa_1\xi_r \\ -2\bar{\alpha}\kappa_1(1/r)\,\xi_\omega \end{pmatrix},$$

$$\begin{aligned} \vartheta &= \mathbf{a}\cdot\xi, & \delta_1 &= (\gamma - 1), \\ \eta &= (\delta_1/2)\,|\,\mathbf{a}\,|^2, & \delta_2 &= (\gamma - 2), \\ \omega &= -\gamma(e/\rho) + 2\eta, & \delta_3 &= (\gamma - 3). \end{aligned} \tag{A2}$$

γ gives the ratio of the specific heats. The components of the inverses of $t_{m+1/2}$ are

$$\begin{aligned}
\tau_{11} &= \delta_1[|\,\psi\,|^2 + (\omega - \eta)|\,\xi\,|^2] + (\gamma + 1)\,\vartheta^2, \\
\tau_{12} &= -\delta_1\epsilon_1 - \gamma\vartheta\xi_1, \\
\tau_{13} &= -\delta_1\epsilon_2 - \gamma\vartheta\xi_2, \\
\tau_{14} &= -\delta_1\epsilon_3 - \gamma\vartheta\xi_3, \\
\tau_{15} &= \delta_1\,|\xi\,|^2, \\
\tau_{21} &= \eta\xi_1 + \vartheta(-\delta_1\zeta_1 + \gamma a_1\vartheta - \xi_1\chi), \\
\tau_{22} &= \delta_1\psi_1{}^2 + \gamma\vartheta(a_2\xi_2 + a_3\xi_3) - (\xi_2{}^2 + \xi_3{}^2)\chi, \\
\tau_{23} &= \tau_{32} + \gamma\vartheta\psi_3, \\
\tau_{24} &= \tau_{42} - \gamma\vartheta\psi_2, \\
\tau_{25} &= \delta_1\epsilon_1, \\
\tau_{31} &= \eta\epsilon_2 + \vartheta(-\delta_1\zeta_2 + \gamma a_2\vartheta - \xi_2\chi), \\
\tau_{32} &= \delta_1\psi_1\psi_2 - \gamma\vartheta a_2\xi_1 + \xi_1\xi_2\chi, \\
\tau_{33} &= \delta_1\psi_2{}^2 + \gamma\vartheta(a_1\xi_1 + a_3\xi_3) - (\xi_1{}^2 + \xi_3{}^2)\chi, \\
\tau_{34} &= \tau_{43} + \gamma\vartheta\psi_1, \\
\tau_{35} &= \delta_1\epsilon_2, \\
\tau_{41} &= \eta\epsilon_3 + \vartheta(-\delta_1\zeta_3 + \gamma a_3\vartheta - \xi_3\chi), \\
\tau_{42} &= \delta_1\psi_1\psi_3 - \gamma\vartheta a_3\xi_1 + \xi_1\xi_3\chi, \\
\tau_{43} &= \delta_1\psi_2\psi_3 - \gamma\vartheta a_3\xi_2 + \xi_2\xi_3\chi, \\
\tau_{44} &= \delta_1\psi_3{}^2 + \gamma\vartheta(a_1\xi_1 + a_2\xi_2) - (\xi_1{}^2 + \xi_2{}^2)\chi, \\
\tau_{45} &= \delta_1\epsilon_3, \\
\tau_{51} &= (\eta - \omega)(\eta\,|\,\xi\,|^2 - \delta_2\vartheta^2), \\
\tau_{52} &= \delta_1[(\omega - \eta)\,\epsilon_1 + \vartheta\zeta_1] + \xi_1\vartheta\omega, \\
\tau_{53} &= \delta_1[(\omega - \eta)\,\epsilon_2 + \vartheta\zeta_2] + \xi_2\vartheta\omega, \\
\tau_{54} &= \delta_1[(\omega - \eta)\,\epsilon_3 + \vartheta\zeta_3] + \xi_3\vartheta\omega, \\
\tau_{55} &= \delta_1\,|\,\psi\,|^2 - (\omega - \eta)|\,\xi\,|^2 + \vartheta^2,
\end{aligned} \tag{A3}$$

$\det\,|\,t\,| = \Delta = \vartheta[\delta_1\,|\,\psi\,|^2 - \chi\,|\,\xi\,|^2 + \gamma\vartheta^2]$.

$$\begin{pmatrix} \psi_1 \\ \psi_2 \\ \psi_3 \end{pmatrix} = \psi = \xi \times \mathbf{a}, \qquad \begin{pmatrix} \zeta_1 \\ \zeta_2 \\ \zeta_3 \end{pmatrix} = \zeta = \psi \times \mathbf{a},$$

$$\begin{pmatrix} \epsilon_1 \\ \epsilon_2 \\ \epsilon_3 \end{pmatrix} = \epsilon = \psi \times \xi, \qquad \chi = (\gamma\eta - \delta_1\omega). \tag{A4}$$

APPENDIX B

If we select from the total of six equations Eqs. (4.2) and (4.1), the first four components of Eqs. (4.2) and additionally Eq. (4.1) to calculate the five unknowns ρ_m, $\mathbf{m}_m$, e_m, the system of equations indicated below is free from undefined terms of the type 0/0 which cannot be processed in a numerical computation:

$$
\begin{aligned}
e_m &= \frac{\sigma_6\sigma_1 - \sigma_3\sigma_4}{\sigma_5\sigma_1 - \sigma_2\sigma_4}, \\
m_{3;m} &= \frac{\sigma_3 - e_m\sigma_2}{\sigma_1}, \\
m_{2;m} &= \frac{t_\delta - m_{3;m}t_\beta - e_m t_\gamma}{t_\alpha}, \\
m_{1;m} &= \frac{1}{\xi_1}\,[f_1^* - \xi_2 m_{2;m} - \xi_3 m_{3;m}, \\
\rho_m &= \frac{t_f - e_m\xi_1 t_{35} - m_{3;m}t_e - m_{2;m}t_d}{\xi_1 t_{31}};
\end{aligned}
\tag{B1}
$$

$$
\begin{aligned}
\sigma_1 &= t_\mu t_\alpha - t_\beta t_\epsilon \\
\sigma_2 &= t_\nu t_\alpha - t_\gamma t_\epsilon \\
\sigma_3 &= t_\eta t_\alpha - t_\delta t_\epsilon \\
\sigma_4 &= t_\vartheta t_\alpha - t_\beta t_\xi \\
\sigma_5 &= t_\tau t_\alpha - t_\gamma t_\xi \\
\sigma_6 &= t_\omega t_\alpha - t_\delta t_\xi
\end{aligned}
\tag{B2}
$$

$$
\begin{aligned}
t_\alpha &= t_{21}t_d - t_{31}t_a, & t_\nu &= t_{21}t_{45} - t_{41}t_{25}, \\
t_\beta &= t_{21}t_e - t_{31}t_b, & t_\eta &= t_{21}t_i - t_{41}t_c, \\
t_\gamma &= t_{21}t_{35} - t_{31}t_{25}, & t_\xi &= t_{21}t_k - \mu_{1;m}t_a, \\
t_\delta &= t_{21}t_f - t_{31}t_c, & t_\vartheta &= t_{21}t_l - \mu_{1;m}t_b, \\
t_\epsilon &= t_{21}t_g - t_{41}t_a, & t_\tau &= t_{21}\mu_{5;m} - \mu_{1;m}t_{25}, \\
t_\mu &= t_{21}t_h - t_{41}t_b, & t_\omega &= t_{21}t_0 - \mu_{1;m}t_c, \\
t_a &= \xi_1 t_{23} - t_{22}\xi_2, & t_g &= \xi_1 t_{43} - t_{42}\xi_2, \\
t_b &= \xi_1 t_{24} - t_{22}\xi_3, & t_h &= \xi_1 t_{44} - t_{42}\xi_3, \\
t_c &= \xi_1 f_2^* - t_{22}f_1^*, & t_i &= \xi_1 f_4^* - t_{42}f_1^*, \\
t_d &= \xi_1 t_{33} - t_{32}\xi_2, & t_k &= \xi_1\mu_{3;m} - \mu_{2;m}\xi_2, \\
t_e &= \xi_1 t_{34} - t_{32}\xi_3, & t_l &= \xi_1\mu_{4;m} - \mu_{2;m}\xi_3, \\
t_f &= \xi_1 f_3^* - t_{32}f_1^*, & t_0 &= \xi_1 g_m - \mu_{2;m}f_1^*.
\end{aligned}
$$

The t_{ij} $(i, j = 1,..., 5)$ are the components of $t_{m+1/2}$, Eqs. (A1). From Eqs. (4.2) we obtain, further,

$$f^{*n+(j/2)}_{m+1/2} = \begin{pmatrix} f^*_1 \\ f^*_2 \\ f^*_3 \\ f^*_4 \\ f^*_5 \end{pmatrix}^{n+(j/2)}_{m+1/2} = f^{n+(j/2)}_{m+1/2} - s^{n+(j/2)}_{m+1/2} U^{n+(j+1)}_{m+1,l}. \tag{B3}$$

REFERENCES

1. M. D. VAN DYKE, *J. Aeronaut. Sci.* **25** (1958), 485.
2. P. R. GARABEDIAN AND H. M. LIEBERSTEIN, *J. of Aeronaut. Sci.* **25** (1958), 109.
3. A. N. LYUBIMOW AND V. V. RUSANOW, NASA TT F-714, 1973.
4. G. MORETTI AND G. BLEICH, *AIAA J.* **5** (1967), 1557.
5. C. WEILAND, ESA TT-268, 1975.
6. K. OBERLÄNDER, Ph.D. Thesis, Ruhr-Universität Bochum, Germany, 1974.
7. A. W RIZZI AND M. INOUYE, *AIAA J.* **11** (1973), 1478.
8. C. WEILAND, DLR-FB 76-65, 1976.
9. D. RUES, *Z. Angew. Math. Mech.* **52** (1972), 497.
10. P. D. THOMAS, R. A. VINOKUR, R. A. BASTIANON, AND R. J. CONTI, *AIAA J.* **10** (1972), 887.
11. C. WEILAND, *ZFW* **24** (1976), 237.
12. C. WEILAND, DLR-FB 76-57, 1976.
13. K. FÖRSTER, K. ROESNER, AND C. WEILAND, "Lecture Notes in Physics," Vol. 35, p. 167, Springer-Verlag, Berlin, 1975.
14. K. I. BABENKO, G. P. VOSKRESENSKII, A. N. LYUBIMOW, AND V. V. RUSANOW, "Three-Dimensional Flow of Ideal Gas around Smooth Bodies," translated from Russian by Israel Program for Scientific Translations, Jerusalem, 1968.
15. M. VINOKUR, NASA TM-X 62, 415, 1974.
16. M. VINOKUR, *J. Computational Physics* **14** (1974), 105.
17. G. MORETTI, B. GROSSMAN, AND F. MARCONI, AIAA Paper No. 72-192, 1972.
18. P. J. ROACHE, "Computational Fluid Dynamics," Hermosa, Albuquerque, N.M., 1972.
19. P. D. LAX, *Comm. Pure Appl. Math.* **7** (1954), 159.
20. P. D. LAX AND B. WENDROFF, *Comm. Pure Appl. Math.* **13** (1960), 217.
21. P. D. LAX AND B. WENDROFF, *Comm. Pure Appl. Math.* **19** (1964), 473.
22. R. W. MACCORMACK AND A. J. PAULLAY, AIAA Paper No. 72-154, 1972.
23. P. KUTLER, "Computation of Three-Dimensional Inviscid Supersonic Flows," Short Course of v. Karman Institut, Rhode-Saint-Genese, Belgium, 1975.
24. P. KUTLER, H. LOMAX, AND R. F. WARMING, AIAA Paper No. 72–193, 1972.
25. P. KUTLER, W. A. REINHARDT, AND R. F. WARMING, *AIAA J.* **11** (1973), 637.
26. M. J. ABBETT, Aerotherm. Corp., Mt. View, Calif., Final Rep. 71-41, 1971.
27. R. M. BEAM AND R. F. WARMING, *J. Computational Physics* **22** (1976), 87.
28. R. COURANT AND D. HILBERT, "Methoden der Mathematischen Physik," Springer-Verlag, Berlin, 1968.
29. C. WEILAND AND H.-J. THIES, DFVLR-FB 78–09, 1978.
30. T. HSIEH, *J. Spacecr. Rockets* **14** (1977), 662.
31. K. HARTMANN, "Drei-Komponenten-und Druckverteilungsmessungen einschließlich Strömungsbeobachtungen an einem kreiszylindrischen Flugkörperrumpf mit verschiedenen Kopfformen bei Machzahlen $M_\infty = 0.5$ bis 2.2 und verschiedenen Reynoldszahlen," Internal Report of the Deutsche Forschungs- und Versuchsanstalt für Luft- und Raumfahrt, Rep. No. 251 74A32, 1974.
32. C. V. D. VYLE, "Dreidimensionale Strömungsfelduntersuchungen an einem Flugkörper im Überschall," ERNO Raumfahrttechnik, Report Nr. T/RF 41/RF410/51108 (1976).